Analysis of Nonuniformities in the Plasma Etching of Silicon with CF_4/O_2

Alan S. Kao and Harvey G. Stenger, Jr.

Department of Chemical Engineering, Lehigh University, Bethlehem, Pennsylvania 18015

ABSTRACT

Experimental and modeling work has been performed to examine the effects of reactor pressure, etchant gas flow rate, and wafer location on the uniformity of plasma etching silicon using CF_4/O_2 in a parallel-plate-radial flow reactor. Intrawafer etch rates were measured at 12 points across a 3 in. wafer at pressures between 125 and 200 mtorr, 70°C, and gas residence times between 1.28 and 2.14s. Depending on the operating conditions, an edge-to-center decrease in etch rate of 5-25% was observed. A combined reactor/reaction model is able to predict this degree of nonuniformity. Uniformity was improved by increasing the reactor pressure and decreasing the flow rate of the etchant gas. Etch uniformity was also found to be a function of wafer location within the reactor. Data are presented which show the influences of process parameters on both etch rate magnitude and uniformity.

Intrawafer nonuniform etching in plasma and reactive ion etching systems is a major problem in current IC processing technology. The result of intrawafer nonuniformities is a direct decrease in circuit yields or overdesign to compensate for etch rate variations. In particular, the plasma etching of silicon, silicon dioxide, and aluminum in a parallel plate radial flow system often displays an edge-to-center decrease in etch rate, a phenomenon sometimes referred to as the "bullseye effect" (1, 2). Clearly, the inability to etch consistent circuits on each chip of a wafer will continue unless the causes of the bullseye effect are better understood and corrections are made.

Several papers have been published which discuss the problem of etch nonuniformities. Stenger *et al.* (1) studied the interwafer nonuniformities of NF_3 etching silicon in a radial flow reactor. The etch rates for this system were found to be more uniform at lower flow rates holding pressure, feed gas composition, and temperature constant. Since they evaluated etch rates by measuring the decrease in wafer mass after etching, intrawafer nonuniformities could not be examined. Dalvie *et al.* (3) have developed a model of CF_4 etching silicon in a radial flow reactor. Their model assumes uniformly distributed silicon on the lower electrode, low CF_4 dissociation rates, and radially constant electron density. The effects of pressure, flow rate, and discharge power on etch rate were simulated. They found that average etch rates increased as the flow rate decreased or the reactor pressure increased. The primary effect of increasing the discharge power in their model was to increase the average electron density, which resulted in higher etch rates. Their model also predicted intrawafer as well as interwafer etch nonuniformities; however, no experimental data were offered for comparison. Alkire and Economou (4) examined the nonuniform stripping of photoresist with O_2 in a barrel reactor, which is a common application of barrel etchers. The transport of etching species to the wafer in barrel reactors relies predominantly on diffusion, with little convective influences. This results in a depletion of the etching species across the wafer, thus causing nonuniform etching. Again, only model results were given with no experimental data. Experimental work has been published by Nagy (2) and Peccoud *et al.* (5). Nagy presented an experimental investigation of reactive ion etch nonuniformities. He attributed the decrease in etch rate from edge to center to an intensified production of the reactant species over the wafer. Peccoud *et al.* also observed the bullseye effect when etching aluminum with CCl_4 in a parallel plate reactor, which they minimized experimentally by increasing the RF frequency.

This paper presents the results of a series of experiments aimed at quantifying the dependencies of etch uniformity on process parameters. Data are presented showing the effects of reactor pressure, etchant gas flow rate, and wafer location on the intrawafer etch profile uniformity. These data were taken from a parallel-plate radial-flow plasma etching reactor (RFPER). A quantitative model is also developed which helps explain several trends in the data.

Experimental

The data presented were obtained using a Plasma-Therm (P.T.) PK-2440 RFPER similar to that used in our previous work (1). A schematic diagram of the RFPER is shown in Fig. 1. A radio frequency (RF) generator (P.T. Model HFS-3000D) feeds a 13.56 MHz signal to the upper electrode while the lower electrode is grounded. A matching network (P.T. Model AMNS-3000E) is used to match the impedance of the plasma process to that of the RF generator. Both electrodes are 55.9 cm diam, the exit port is 5.8 cm diam, and an electrode spacing of 5.7 cm was used for our experimental work. A heat exchanger (P.T. Model HES-1), controlled by a temperature regulator (P.T. Model TR-1), is used to control the lower electrode temperature. The upper electrode is not heated.

The etchant gas used was a commercially available mixture of 4% O_2 in CF_4 (Matheson Gas). CF_4 is an etchant gas commonly used for etching semiconductors and metals (6, 7) and O_2 is added to improve etch rate (8). The gas enters the reactor at the outer edge of the electrode through a perforated tube and flows axisymmetrically toward the exit port in the center. Three inch diameter silicon wafers were placed on the lower electrode in various configurations. Prior to etching the wafers, a 5000Å layer of thermal silicon dioxide was grown on the <100> face. The wafers were subsequently patterned using Baker PR-1 positive photoresist and the exposed SiO_2 was wet etched with HF to leave 20% of the surface area as bare silicon. The resist was then removed with acetone, leaving the other 80% of the wafer surface as silicon dioxide. The wafers were pat-

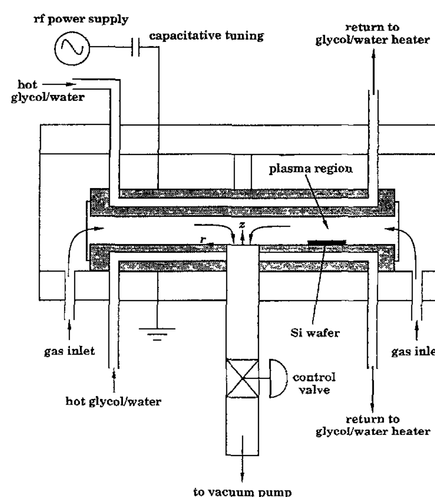

Fig. 1. Schematic diagram of the radial flow plasma etching reactor for etch rate measurements.

DOCKET ALARM Find authenticated court documents without watermarks at docketalarm.com.

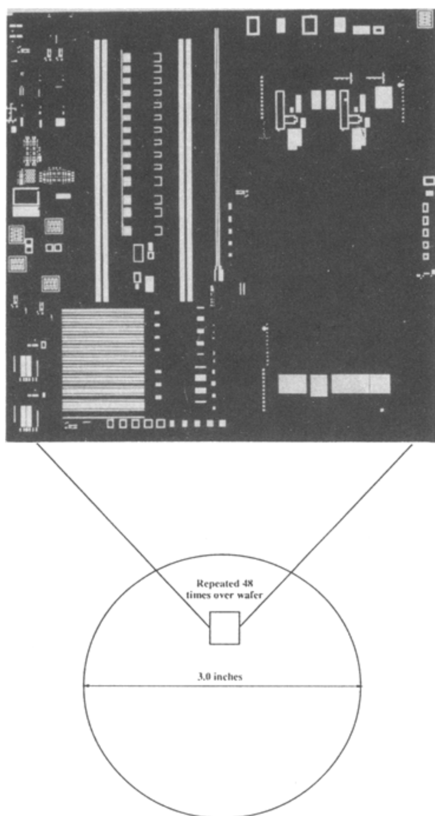

Fig. 2. Silicon dioxide mask pattern used to define regions to be etched.

terned to allow measurement of etch depths continuously across the wafer. Figure 2 diagrams the etched pattern.

Etch depths were measured at various stages of the experimental process: (*i*) before etching, to measure the initial SiO_2 film thickness, (*ii*) immediately after etching, to measure the amount of SiO_2 and silicon that was removed, and (*iii*) after stripping off the oxide layer with HF, to determine the amount of silicon etching that had occurred. The etch depths were measured using a Sloan Dektak surface profile measuring system. Etch rates were calculated as etch depth of silicon divided by etch time.

The flow of the etchant gas is regulated by a mass flow controller unit (MKS Instruments Model 254), which is capable of providing constant flow rates up to 100 sccm. The pressure in the reactor chamber is maintained by a pressure monitor (P.T. Model PRM-1) and a process valve controller (P.T. Model PVC-3). This pressure control system can maintain pressures from 50-1000 mtorr at an inlet flow of 100 sccm.

The base operating conditions were a reactor pressure of 150 mtorr, an electrode temperature of 70°C, and an etchant gas flow rate of 100 sccm. Heat transfer rates are adequate in this reactor configuration (10) to allow the assumption of isothermality for the electrode, the gas neutral species, and the wafer. Etch times were 15 min and an RF power of 750W (0.31 W/cm² or 0.054 W/cm³) was used. To increase the reproducibility of the results, the reactor system was conditioned before each set of experiments by etching a series of bare silicon wafers as a blank run. The chamber was thoroughly purged several times with nitrogen before feeding with CF_4/O_2.

Experimental Results

Radial etch profiles were measured from the point closest to the reactor exit (point A) to the point closest to the reactor entrance (point B) for several wafer configurations. The data are plotted in two ways: (*i*) average absolute etch rate at any position across the wafer, and (*ii*) etch rates normalized to the minimum etch rate over the wafer, to indicate the degree of nonuniformity across each wafer. The etch rates in Fig. 3-6 were measured at twelve locations across the wafer diameter. Smooth curve etch profiles were determined by a second-order regression and are plotted on each figure to help visualize the data trends. In all of these experiments, the amount of SiO_2 etching that occurred was negligible compared to the amount of silicon removed.

The first series of experiments involved the etching of a single wafer at a time. The wafer was placed in the center radial location (see insert in Fig. 3) and etched using the base case conditions and gas flow rates of 60, 80, and 100 sccm. The resulting etch rate profiles are shown in Fig. 3. The etch rate was highest at the point closest to the reactor exit (point A) in all cases. The data plotted on the normalized scale in Fig. 3 show that etching becomes more uniform with decreasing flow rate. The relative difference between the highest and lowest etch rate across each wafer dropped from 15 to 3% as the flow rate was decreased from 100 to 60 sccm. The absolute etch rate scale in Fig. 3 shows that the average etch rate decreases from 2790 to 2480 A/min with decreasing flow rate.

The effects of varying the reactor pressure from 125 to 150 to 200 mtorr at constant flow rate and temperature are shown in Fig. 4. As pressure is increased, the uniformity of the etching improves; the relative difference between each wafer's highest and lowest etch rate went from 15 down to 5% as the pressure was increased from 125 to 200 mtorr. The average absolute etch rate increases from 2450 to 2600 A/min with increasing pressure from 125 to 200 mtorr.

Figure 5 shows the effect of wafer location on the intrawafer etch profile. In separate runs, individual wafers were etched in each of the three positions shown as inserts on Fig. 5. The reaction conditions were those of the base case (100 sccm, 150 mtorr, 70°C, and 750W). The etch nonuniformity is similar for the three wafers; all three show a steady increase in etch rate in the direction of the flow. The average etch rate of the wafers decreased from 2690 to 2480 to 2290 A/min for the outer-, center-, and inner-placed wafers, respectively.

Loading the reactor with three wafers at once (see insert of Fig. 6) resulted in an almost uniform etch profile for the wafer closest to the reactor entrance (Fig. 6). The relative difference in etch rate across the wafer was only 3%. The wafer at the inner position displayed a nonuniform etch rate profile similar to that obtained in the experiment with only one wafer at the inner position. However, the relative difference in etch rate across the inner-placed wafer increased to 25% from the 11% difference obtained when the wafer was etched alone in the inner position. A "loading effect" (10, 11) is observed in Fig. 6 since the average etch

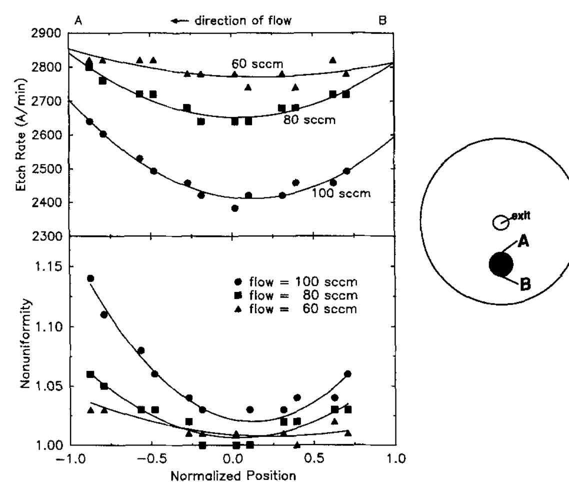

Fig. 3. Effects of flow rate on etch rate and etch uniformity. Pressure = 150 mtorr, temperature = 70°C, RF power = 750W. Data points are measured values, and curves are second-order polynomials fit to the data.

DOCKET ALARM Find authenticated court documents without watermarks at docketalarm.com.

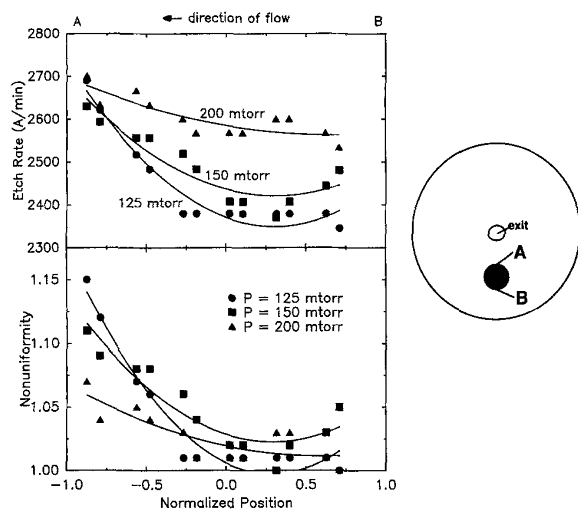

Fig. 4. Effects of reactor pressure on etch rate and etch uniformity. Flow rate = 100 sccm, temperature = 70°C, RF power = 750W. Data points are measured values and curves are second-order polynomials fit to the data.

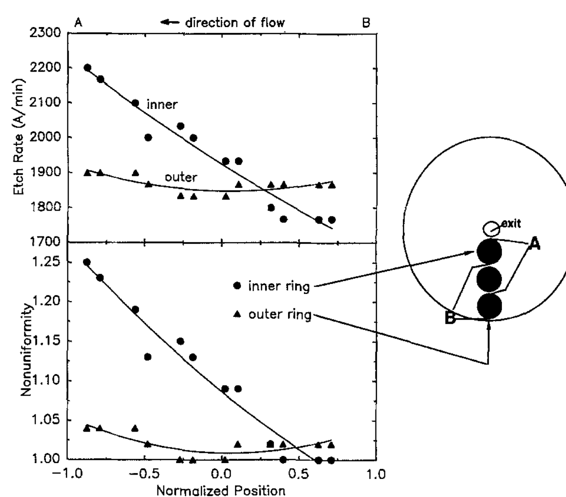

Fig. 6. Effects of wafer loading on etch rate and etch uniformity. Pressure = 150 mtorr, flow rate = 100 sccm, temperature = 70°C, RF power = 750W. Data points are measured values, and curves are second-order polynomials fit to the data.

rate of these wafers (1900-2000 A/min) is significantly lower than that of a single wafer run at the same conditions (2480 A/min).

Discussion

The observed nonuniformities in etch rate provide a good test for any quantitative model which attempts to explain the concentration profiles within a plasma reactor. Modeling the plasma etching process is an interesting problem because of the complexities of the plasma system. An accurate model for predicting the concentration profile of any species within the reactor must account for changes in concentration due to diffusion, convection, and chemical reaction.

In the past, there have been several models describing the plasma etching process. Models for radial flow reactors have been presented for CF_4 by Dalvie *et al.* (3), SF_6 by Kline (12), SF_6/O_2 by Anderson *et al.* (13), and NF_3 by Stenger *et al.* (1). Kushner (14) developed a general model using a parallel plate configuration for the etching of Si and SiO_2 in C_nF_m/H_2 and C_nF_m/O_2 plasmas. Lii *et al.* (15) combined an analog circuit model to predict the electron energy and electron density with a kinetic model for SF_6 etching silicon. Edelson and Flamm (16) simulated CF_4 etching silicon using a cylindrical plug flow configuration and Alkire and Economou (4) presented a model for the nonuniform stripping of photoresist with O_2 in a barrel reactor. While some of these papers have discussed the problem of intrawafer nonuniform etching, little experimental data have been published and compared to the derived models.

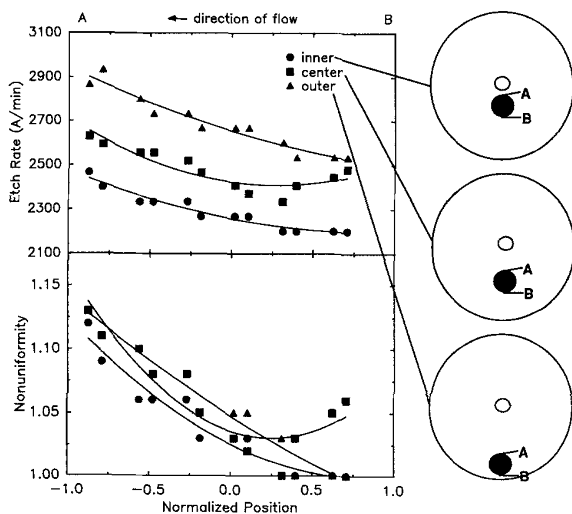

Fig. 5. Effects of wafer position on etch rate and etch uniformity. Pressure = 150 mtorr, flow rate = 100 sccm, temperature = 70°C, RF power = 750W. Data points are measured values, and curves are second-order polynomials fit to the data.

Model Development

In contrast to the more complex models that have been presented by others (3, 13, 16, 17), the model presented here takes a simplified approach to the plasma etching system. Although we recognize the complexity of plasma etching, it is expected that much can be learned from a simplified model that explains a majority of the observations. Therefore our objective is to present a model which helps to explain experimental data without introducing unnecessary complexity.

The model will assume that plasma etching occurs via three lumped reaction steps: (*i*) dissociation of etchant gas molecules by electron bombardment (or chemical reaction with free radicals) (18); followed by (*ii*) a surface reaction between the substrate atoms and the reactive etching species produced in the plasma, and (*iii*) chemically reactive species (free radicals) recombining to form nonreactive species through loss reactions. The surface reaction may be further broken down to adsorption of the etching species, surface reaction, and desorption of the resulting volatile molecules into the plasma.

Of equal importance to these reaction steps are the diffusion and convection of species within the reactor. Therefore, the concentration of the etching species at any location in the reactor is governed by: (*i*) generation by electron dissociation and chemical reaction of etchant gas molecules, (*ii*) losses due to reaction with the substrate material, (*iii*) losses due to free radical reactions, (*iv*) diffusion into and from other regions, and (*v*) convective influences due to gas flow from the reactor entrance to exit.

It is assumed here that the etching species are predominantly generated in the plasma when collisions between electrons and the etchant gas molecules produce reactive ions and free radicals. In the present system, electron collisions with CF_4 molecules most probably produce CF_3 and F radicals. It is also known that the reaction $CF_4 + e^- \rightarrow CF_2 + 2F$ (18) occurs appreciably; however, our method would determine, as in our previous work (1), that the reaction rate constant found from the experimental data would be a product of the dissociation rate constant and the stoichiometric coefficient of the fluorine produced

DOCKET ALARM Find authenticated court documents without watermarks at docketalarm.com.

in the dissociation rate. It can also be expected that the dissociation reaction is directly related to the concentration of electrons and their energy distribution (which is dependent on the power supplied to the electrode and the reactor pressure) (19) and the fluorinated species concentration. Although Plumb and Ryan (18) show that F radicals can also be formed by oxygen reactions, we are at much lower O_2 concentrations than in their work [4% here *vs.* 25% in (18)]. We therefore ignore the contribution of oxygen on the generation of F radicals.

The surface reaction between fluorine atoms and silicon has been studied in depth by Flamm *et al.* (17, 20). In their mechanism, the exposed silicon surface is perfluorinated with adsorbed fluorine, followed by SiF_2 molecules desorbing due to further collisions of the substrate with fluorine atoms. The desorbed SiF_2 perfluorinates rapidly in the plasma to form stable SiF_4. As a result of the etching reaction, there is a decrease in fluorine concentration in regions close to the silicon surface. This creates a concentration gradient, causing fluorine atoms in nonetching regions of the reactor to diffuse toward the wafer.

Recombination or loss reactions (producing F_2, C_2F_6, COF, F_2O, or reproducing CF_4) are numerous (18). To develop a detailed model which includes each reaction would require increased computational difficulties with little difference in the final results. For the present model, it is assumed that the amount of F consumed by loss reactions is first order in F and first order in gas density, since nearly all gas phase species can react with fluorine radicals to form a nonreactive species.

Designating k^*_d to be the rate constant for the dissociation of CF_4, k_e to be the rate constant for the surface etching reaction, and k_l to be the loss reaction rate constant, the rate of reaction in the gas phase (positive for appearance and negative for disappearance) of each major component can be written

$$\text{Fluorine:} \quad r_F = +k^*_d c_{CF_4} c_{e^-} - k_e c_F a_{Si} - k_l c_F \frac{P}{RT} \qquad [1a]$$

$$CF_4\text{:} \quad r_{CF_4} = -k^*_d c_{CF_4} c_{e^-} \qquad [1b]$$

$$\text{Silicon:} \quad r_{Si} = +\frac{1}{4} k_e c_F a_{Si} \qquad [1c]$$

Replacing $k^*_d c_{e^-}$ with k_d, the component continuity equations for CF_4 and F are

$$CF_4\text{:} \quad v_r \frac{\partial c_{CF_4}}{\partial r} = D_{CF_4\text{-}CF_4} \left\{ \frac{1}{r}\frac{\partial}{\partial r}\left(r \frac{\partial c_{CF_4}}{\partial r}\right) + \frac{1}{r^2}\frac{\partial^2 c_{CF_4}}{\partial \theta^2} + \frac{\partial^2 c_{CF_4}}{\partial z^2} \right\} - k_d c_{CF_4} \qquad [2a]$$

$$F\text{:} \quad v_r \frac{\partial c_F}{\partial r} = D_{F\text{-}CF_4} \left\{ \frac{1}{r}\frac{\partial}{\partial r}\left(r \frac{\partial c_F}{\partial r}\right) + \frac{1}{r^2}\frac{\partial^2 c_F}{\partial \theta^2} + \frac{\partial^2 c_F}{\partial z^2} \right\} + k_d c_{CF_4} - k_l c_F \frac{P}{RT} \qquad [2b]$$

In Eq. [2a-b] the gas is assumed to be primarily composed of CF_4 species. Both component balances must be solved simultaneously since the generation of F is dependent on the concentration of CF_4. It is assumed here that the concentration of electrons is only a function of the power supplied to the electrodes, independent of location, and that the effects of pressure and gas flow rate on electron concentration are negligible.

In previous work for this reactor configuration (1), the concentration of reacting species was shown to be only slightly dependent on z. The etching rates, pressures, and dimensions are similar in this work; therefore, the concentrations and their derivatives can be replaced by the average across the reactor thickness

$$\bar{c}_i \equiv \frac{1}{2h} \int_{-h}^{h} c_i dz \qquad [3]$$

Assuming that the derivatives of concentration with respect to r and θ are independent of z, these derivatives can be removed from the integrals in Eq. [2a-b]. Substituting the definition of Eq. [3] and [2a-b] and integrating gives

$$\bar{v}_r \frac{\partial \bar{c}_{CF_4}}{\partial r} = D_{CF_4\text{-}CF_4} \left\{ \frac{1}{r}\frac{\partial}{\partial r}\left(r \frac{\partial \bar{c}_{CF_4}}{\partial r}\right) + \frac{1}{r^2}\frac{\partial^2 \bar{c}_{CF_4}}{\partial \theta^2} + \frac{1}{2h}\left(\frac{\partial c_{CF_4}}{\partial z}\right)_{z=h} - \frac{1}{2h}\left(\frac{\partial c_{CF_4}}{\partial z}\right)_{z=-h} \right\} - k_d \bar{c}_{CF_4} \qquad [4a]$$

$$\bar{v}_r \frac{\partial \bar{c}_F}{\partial r} = D_{F\text{-}CF_4} \left\{ \frac{1}{r}\frac{\partial}{\partial r}\left(r \frac{\partial \bar{c}_F}{\partial r}\right) + \frac{1}{r^2}\frac{\partial \bar{c}_F}{\partial \theta^2} + \frac{1}{2h}\left(\frac{\partial c_F}{\partial z}\right)_{z=h} - \frac{1}{2h}\left(\frac{\partial c_F}{\partial z}\right)_{z=-h} \right\} + k_d \bar{c}_{CF_4} - k_l \bar{c}_F \frac{P}{RT} \qquad [4b]$$

It is assumed the derivatives with respect to z are not functions of z except at the surface of the wafer. Where there is exposed silicon, there will be a flux of fluorine atoms as they adsorb onto the wafer surface and subsequently react. This flux is represented by

$$D_{F\text{-}CF_4} \left(\frac{\partial c_F}{\partial z}\right)_{z=-h} = S(r, \theta) k_e \bar{c}_F \qquad [5]$$

where the function $S(r, \theta)$ is equal to the fraction of the wafer's silicon exposed to the plasma at the surface of the wafer and zero everywhere else. The mask pattern used is assumed to be uniform and has line spacings which are much less than the electrode spacing. Therefore, instead of devising a complex function for describing the position of the lines being etched on the wafer, we have chosen to use the function S to indicate where the flow of F atoms normal to the electrode mostly occurs. The SiO_2 mask used experimentally covered 80% of the wafer surface. By setting $S = 0.2$ over the entire wafer, we imply that etching occurring over the available silicon area, which is 20% of the total wafer area, can be approximated by simulating etching over the entire wafer surface area at 20% of the actual etch rate.

Since the z dependence of concentrations has been removed, it can be assumed that at all values of z other than where there is etchable material, the flux in the z direction is zero

$$D_{F\text{-}CF_4} \left(\frac{\partial c_F}{\partial z}\right)_{z=h} = D_{CF_4\text{-}CF_4} \left(\frac{\partial c_{CF_4}}{\partial z}\right)_{z=\pm h} = 0 \qquad [6]$$

Substituting Eq. [5] and [6] as well as the relationship $\bar{v}_r = \bar{v}_0 r_o / r$ from the overall continuity equation into Eq. [4a-b]

$$\frac{\bar{v}_0 r_o}{r} \frac{\partial \bar{c}_{CF_4}}{\partial r} = D_{CF_4\text{-}CF_4} \left\{ \frac{1}{r}\frac{\partial}{\partial r}\left(r \frac{\partial \bar{c}_{CF_4}}{\partial r}\right) + \frac{1}{r^2}\frac{\partial^2 \bar{c}_{CF_4}}{\partial \theta^2} \right\} - k_d \bar{c}_{CF_4} \qquad [7a]$$

$$\frac{\bar{v}_0 r_o}{r} \frac{\partial \bar{c}_F}{\partial r} = D_{F\text{-}CF_4} \left\{ \frac{1}{r}\frac{\partial}{\partial r}\left(r \frac{\partial \bar{c}_F}{\partial r}\right) + \frac{1}{r^2}\frac{\partial^2 \bar{c}_F}{\partial \theta^2} \right\} - \frac{S k_e}{2h} \bar{c}_F + k_d \bar{c}_{CF_4} - k_l \bar{c}_F \frac{P}{RT} \qquad [7b]$$

In dimensionless form, these equations become

$$\frac{Pe_{CF_4}}{\xi} \frac{\partial C_{CF_4}}{\partial \xi} = \frac{1}{\xi}\frac{\partial}{\partial \xi}\left(\xi \frac{\partial C_{CF_4}}{\partial \xi}\right) + \frac{1}{\xi^2}\frac{\partial^2 C_{CF_4}}{\partial \theta^2} - Bi_d C_{CF_4} \qquad [8a]$$

DOCKET ALARM Find authenticated court documents without watermarks at docketalarm.com.

$$\frac{\gamma \mathrm{Pe}_{CF_4}}{\xi}\frac{\partial C_F}{\partial \xi} = \frac{1}{\xi}\frac{\partial}{\partial \xi}\left(\xi \frac{\partial C_F}{\partial \xi}\right) + \frac{1}{\xi^2}\frac{\partial^2 C_F}{\partial \theta^2} - S\mathrm{Bi}_e C_F + \gamma \mathrm{Bi}_d C_{CF_4} - \mathrm{Bi}_l C_F \quad [8b]$$

where

$$C_i = \frac{\bar{c}_i}{\bar{c}_0},\quad \xi = \frac{r}{r_o},\quad \gamma = \frac{D_{CF_4\text{-}CF_4}}{D_{F\text{-}CF_4}},\quad \mathrm{Pe}_{CF_4} = \frac{v_0 r_o}{D_{CF_4\text{-}CF_4}},$$

$$\mathrm{Bi}_d = \frac{k_d r_o^2}{D_{CF_4\text{-}CF_4}},\quad \mathrm{Bi}_e = \frac{k_e r_o^2}{2h D_{F\text{-}CF_4}},\quad \mathrm{Bi}_l = \frac{k_l r_o^2 (P/RT)}{D_{F\text{-}CF_4}}$$

The boundary conditions at the entrance and exit of this system are the Danckwerts boundary conditions, which assume that no reaction occurs after the reactor exit and that the total flux at the entrance of the reactor is equal to the sum of the convective and diffusive fluxes

$$\left(\frac{\partial C_{CF_4}}{\partial \xi}\right)_{\xi = r/r_o} = \left(\frac{\partial C_F}{\partial \xi}\right)_{\xi = r/r_o} = 0 \quad [9a]$$

$$\frac{1}{\mathrm{Pe}_{CF_4}}\left(\frac{\partial C_{CF_4}}{\partial \xi}\right)_{\xi=1} = C_{CF_4} - y_{CF_4,0} \quad [9b]$$

$$\frac{1}{\gamma \mathrm{Pe}_{CF_4}}\left(\frac{\partial C_F}{\partial \xi}\right)_{\xi=1} = C_F \quad [9c]$$

The diffusion of fluorine atoms in the plasma is of primary interest, since they are the etching species. The diffusion coefficients can be estimated from the Chapman-Enskog Eq. [21]

$$D_{F\text{-}CF_4} = \frac{2.88 \times 10^4}{P} \quad [10]$$

$$D_{CF_4\text{-}CF_4} = \frac{1.40 \times 10^4}{P} \quad [11]$$

where P is in pascals and D_{AB} is in cm^2/s.

Model Solutions

Equations [8a-b] were solved using the finite element program TWODEPEP published by IMSL (22). The process parameters used are summarized in Table I. The solution of equations [8a-b] results in a map of CF_4 and F concentrations throughout the reactor. Etch rates across each wafer are calculated from the product of the fluorine concentration, the etching reaction rate constant, k_e, and the silicon loading density, a_{Si}. Plotting the model-generated map of fluorine concentration gives a visual inspection of the expected etch rate profiles. Figure 7 shows a contour plot of the dimensionless F concentration for the case of one wafer being processed at 100 sccm and 150 mtorr.

The unknown reaction rate constants, k_l, k_d, and k_e, were varied in each call to TWODEPEP to allow minimizing the error between the observed and the calculated etch rate. The three runs which varied flow rate (data of Fig. 3) were used to determine the set of three constants. Observed etch rates (data points) *vs.* predicted etch rates (lines) are shown in Fig. 8 for the single-wafer case at three different flow rates. The agreement is good at 60 and 80 sccm flow rates, with a small deviation observed at 100 sccm near the center of the wafer.

The rate constants used to calculate the model curves in Fig. 8 are given in Table II. The calculated Peclet and Biot numbers for these best-fit parameters are listed in Table III for the various cases. These constants are not to be considered fundamental rate parameters. Instead, they are fit parameters which give a mechanistic structure to the plasma reactor model. However, it is interesting to compare these constants to those reported elsewhere (18). In work by Ryan and Plumb (18) at 500 mtorr and 295 K, constants are reported between 10^{-12} and 10^{-16} cm^3/s/molecule for various reactions which consume fluorine (*e.g.*, $F + CF_3 \rightarrow CF_4$). Our value of 1.11×10^{-16} falls within their range, suggesting it is of a reasonable size.

Plumb and Ryan also report a value for the first-order dissociation constant of CF_4, k_d (which is a product of the

Table I. Summary of parameters

Electrode radius	r_o	27.95 cm
Exit tube radius	r_i	2.9 cm
Wafer radius	r_w	3.81 cm
Reactor volume, half thickness	h	2.85 cm
Electrode temperature	T	343 K
Reactor pressure	P	125, 150, and 200 mtorr
Gas flow rate	F	60, 80, and 100 sccm

Table II. Best fit rate parameters

Dissociation	k_d	$0.13 s^{-1}$
Loss	k_l	6.67×10^7 cm^3/s/gmol or 1.11×10^{-16} cm^3/s/molecule
Etching	k_e	305 cm/s

Table III. Dimensionless numbers for best fit parameters

P (Pa)	Flow (sccm)	Pe_{CF_4}	Bi_d	Bi_e	Bi_l
16.6	100	0.422	0.121	24.2	0.176
19.9	60	0.253	0.145	29.0	0.254
19.9	80	0.338	0.145	29.0	0.254
19.9	100	0.422	0.145	29.0	0.254
26.6	100	0.422	0.193	38.7	0.451

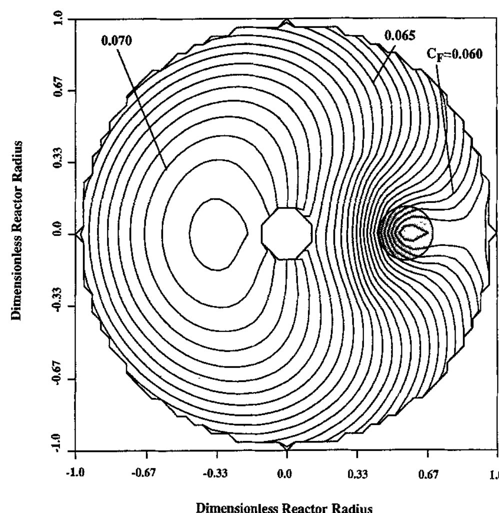

Fig. 7. Contour plot of dimensionless fluorine concentration throughout the reactor. Flow rate = 100 sccm, pressure = 150 mtorr, temperature = 70°C, RF power = 750W.

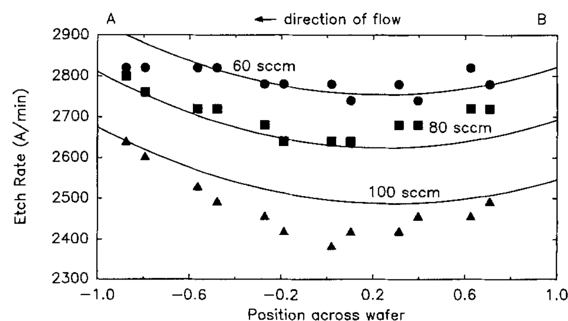

Fig. 8. Model (curves) *vs.* data (points) for the effect of flow rate on etch rate. Pressure = 150 mtorr, temperature = 70°C, RF power = 750W.

DOCKET ALARM Find authenticated court documents without watermarks at docketalarm.com.

DOCKET ALARM

Explore Litigation Insights

Docket Alarm provides insights to develop a more informed litigation strategy and the peace of mind of knowing you're on top of things.

Real-Time Litigation Alerts

Keep your litigation team up-to-date with **real-time alerts** and advanced team management tools built for the enterprise, all while greatly reducing PACER spend.

Our comprehensive service means we can handle Federal, State, and Administrative courts across the country.

Advanced Docket Research

With over 230 million records, Docket Alarm's cloud-native docket research platform finds what other services can't. Coverage includes Federal, State, plus PTAB, TTAB, ITC and NLRB decisions, all in one place.

Identify arguments that have been successful in the past with full text, pinpoint searching. Link to case law cited within any court document via Fastcase.

Analytics At Your Fingertips

Learn what happened the last time a particular judge, opposing counsel or company faced cases similar to yours.

Advanced out-of-the-box PTAB and TTAB analytics are always at your fingertips.

API

Docket Alarm offers a powerful API (application programming interface) to developers that want to integrate case filings into their apps.

LAW FIRMS

Build custom dashboards for your attorneys and clients with live data direct from the court.

Automate many repetitive legal tasks like conflict checks, document management, and marketing.

FINANCIAL INSTITUTIONS

Litigation and bankruptcy checks for companies and debtors.

E-DISCOVERY AND LEGAL VENDORS

Sync your system to PACER to automate legal marketing.

WHAT WILL YOU BUILD? | sales@docketalarm.com | 1-866-77-FASTCASE

fastcase®
Smarter legal research.